JELECHEM-D-08-00106 1st revision

Voltammetric study of adsorption layers of various 4-pyridyl terminated surfactants on a Au(111) electrode: Effects of electronic property of pyridyl group and intermolecular hydrogen bonding upon potential-driven phase changes

Kohei Uematsu[a], Takamasa Sagara[b,*]

Received 15 February 2008
Received in revised form 13 June 2008
Accepted 25 June 2008
Available online 4 July 2008

[a]*Department of Materials Science, Graduate School of Science and Technology, Nagasaki University, Bunkyo 1-14, Nagasaki 852-8521, Japan*
[b]*Department of Applied Chemistry, Faculty of Engineering, Nagasaki University, Bunkyo 1-14, Nagasaki 852-8521, Japan*

[*]Corresponding author. Tel./fax: +81 95 819 2676
E-mail address: sagara@nagasaki-u.ac.jp (T. Sagara)

Abstract

The major factors determining the potential-driven phase changes of the films of 4-pyridyl terminated water-insoluble neutral surfactants on a Au(111) electrode were described using the results of dc and ac voltammetric measurements. In total six surfactants were used to elucidate the effects of electronic property of the 4-pyridyl head group, hydrogen bonding ability between amide groups, direction of the amide bond, and bulkiness around the head group upon the potential dependent reorientation and adsorption-desorption processes. Comparison of the behavior of pentadecyl 4-pyridyl ether **(C15-O-Py**) and 1-pyridin-4-yl-hexadecan-1-one (**C15-(C=O)-Py**), possessing respectively, the highest and lowest excess electronic charge on the pyridyl nitrogen among the six surfactants, revealed that the latter exhibits more distinct reorientation of pyridyl group corresponding to phase transition between condensed and loose-packed states and narrower potential region of the compact film formation. Introduction of amide group in the alkyl chains of the surfactants reduced the packing of the adsorbed film in the potential region of the compact film formation, as evidenced by an increase of the differential capacitance. It was found that the existence of amide group facilitates the potential-driven phase transition of closely packed film from a condensed state to a loosely packed state, whereas it suppresses the transition of loosely packed film. The concomitant steric effect was also discussed.

Keywords: Adsorption-desorption; Au(111) electrode; Organic monolayer; Molecular nano-organization; Potential dependent phase change

1. Introduction

A number of soluble and insoluble surfactants and lipids form their adsorption monolayers as ordered films on metal electrode surfaces through weak attractive interaction with the surfaces. Being driven by the potential change, some of them clearly show dynamic and reversible structural changes including adsorption/desorption, reorientation, and formation/dissolution of the compact film. The potential-driven structural changes of adsorbed films have been so far demonstrated for dodecylsulfonate [1-4], octadecanoic acid [1,5,6], 12-(9-anthroyloxy) stearic acid [7], 1-octadecanol [1,6,8-15], 4-pentadecyl pyridine (**C15-Py**) [1,16-20], phospholipids (dimyristoylphosphatidylcholine and dioleoylphosphatidylcholine) [1,21-29]. Except for the conventional electrochemical methods, used to describe the molecular level details of the structural changes are scanning tunneling microscopy (STM) [2,3,27], atomic force microscopy (AFM) [2], and spectroelectrochemical methods (neutron scattering [4,18,19,28,29], fluorescence [7,9,11,12,15,17,25,30] and IR reflection [13,14,20,24,31] measurements).

Although the potential dependent structures and their dynamic changes have been extensively investigated, little has been reported about the governing factors. It is of profound importance to elucidate the factors of potential-driven, reversible structural changes of adsorbed films from the viewpoint of molecular structure and properties. Using thus obtained factors, one can control the potential induced dynamic behavior by designing the molecular structures of constituent surfactants of the adsorbed films. The potential-driven structural changes may be applicable to the development of a new class of electrochemical devices possessing novel functions. The potential-driven dynamic behavior of the active surfactants depends on adsorbate-substrate interaction, intermolecular interaction, and interplay with solvent. Therefore, one needs to adjust the balance of these multiple interactions in order for fine control the potential-driven behavior to be realized through molecular design.

In the present study, we focus on the electronic property of the head group, intermolecular hydrogen bonding ability between amide groups, and bulkiness as the major factors determining the potential-driven dynamic phase changes of adsorbed films of 4-pyridyl terminated water-insoluble surfactants on a Au(111) electrode surface. The choice

of a 4-pyridyl group as an adsorption functional head group aims at semi-quantitative estimation of the contribution of its interaction with an electrode surface to the potential dependent reorientation and adsorption/desorption. Pyridine is known to exhibit a potential induced reorientation between flat and upright orientations on a Au(111) electrode surface [32-37]. In the upright orientation, a pyridine molecule adsorbs on the electrode surface through the lone-pair electrons at the pyridyl nitrogen with an adsorption energy of 37 kJ mol^{-1} [32-34]. The donation of the lone-pair electrons to the Au surface plays a dominant role when binding to the Au cluster surface as being demonstrated by Wu and coworkers [38].

We expect that the modulation of electronic property of the pyridyl group through molecular structure design changes the affinity of the pyridyl group to the gold electrode surface, leading to a change in the potential-driven behavior of 4-pyridyl terminated surfactants. We, therefore, prepared pentadecyl 4-pyridyl ether (**C15-O-Py**) and 1-pyridin-4-yl-hexadecan-1-one (**C15-(C=O)-Py**) (Scheme 1). Electronic properties of 4-pyridyl groups of these molecules are quite different, because the linker between alkyl chain and 4-pyridyl group is either ether with strong electron-donating ability or carbonyl with strong electron-withdrawing ability. Mutual comparison of the dynamic behavior of these two molecules may enable us to evaluate the effect of the electronic property of pyridyl group on the dynamic behavior, while we must simultaneously take the steric effect of these surfactants as well as the interplay with solvent water into consideration.

Scheme 1

Another important factor to be concerned is intermolecular interaction between adsorbed molecules, especially lateral intermolecular hydrogen bonding between amide groups. We discuss the experimental results for three different amide-containing 4-pyridyl terminated surfactants in Scheme 1.

The effects of the intermolecular hydrogen bonding between amide groups in a self-assembled monolayer (SAM) of an alkanethiol derivative upon the molecular organization structure and its stability have been extensively investigated. Clegg and coworkers prepared a series of SAMs of amide-containing alkanethiols on a Au substrate

[39,40]. Using the results of IR reflection-absorption spectral measurements, they revealed that the amide-containing alkanethiol molecules form extended hydrogen bonding networks and that the existence of amide group disrupts the ordering of the alkyl chains due to the steric effect. They also found that the amide-containing alkanethiol SAM is highly resistant to thermal desorption compared to the amide-free alkanethiol SAM [41]. The increase in thermal stability due to the hydrogen bonding formation was also reported by Vaiokas and coworkers [42]. They found that hydrogen bonds depress the thermal disordering of alkyl chains and that the onset of sulfur desorption takes place at a higher temperature as compared to none hydrogen-bonded analogues. Lewis and coworkers investigated the lattice structure for amide-containing alkanethiol SAMs by STM observation [43]. The structure is mainly of c(4×2) lattice, exhibiting a linear molecular arrangement structure due to the intermolecular hydrogen bonding, in contrast to amide-free normal alkanethiol SAMs. Tam-Chang and coworkers investigated the thermal stability of amide-containing alkanethiol SAMs under an ultrahigh vacuum condition and found that the existence of amide group in the SAM suppresses the desorption of the SAM [44]. Furthermore, the exchange rate of amide-containing short-chain alkanethiols in the SAMs for hexadecanethiol in ethanol solution is 10^2-10^3 times slower than that of an amide-free alkanethiol. They also reported that the introduction of amide group induces conformation changes of the alkyl chains from an all-trans arrangement to gauche containing one.

As described above, even in alkanethiol SAMs, which strongly bind to a Au surface through Au-S covalent bonding with very high adsorption energy, the introduction of amide group into alkanethiol SAMs has a great extent of influence in terms of stability and structure of adsorbed film. Therefore, the introduction of an amide group into a surfactant molecule, which exhibits weak and attractive interaction to a surface, should strongly affect both the potential-driven dynamic behavior and the rigidity of the adsorbed film through lateral intermolecular hydrogen bondings. In dense-packed films of surfactants, hydrogen bonding formation between amide groups may effectively take place. This presumably results in either an increase of rigidity of the compact films as in the case of thermal phase transition reported by Vaiokas [42] or a decrease of rigidity due to both disruption of close-packed alkyl chains and penetration of solvents into adsorbed films.

We previously investigated the effects of the existence of an amide group as the linker

between alkyl chain and pyridyl group and its linking direction upon the potential-driven dynamic behavior [45]. We found that the existence of an amide group and its linking direction significantly affect the behavior of adsorbed films. In the molecules used in our previous work, however, direct connection of the amide group to 4-pyridyl group significantly modified the electronic properties of the head group. Hence, we could not exclusively evaluate the effect of the introduction of amide group. In the present work, we newly use *N*--myristoyl-2-(4-pyridinyl)ethylamine (**C13-CONH-C2Py**) and *N*-tridecyl-*β*-(4-pyridyl)-propionamide (**C13-NHCO-C2Py**) (Scheme 1). Amide groups in these molecules are separated from the pyridyl group by an ethylene linkage. This enables us to keep the electronic property of pyridyl group almost the same as that of **C15-Py**. Comparison among the behavior of these three different surfactants may reveal the effects of existence and direction of amide bond.

In the present paper, we describe the effects of the electronic property of a pyridyl group and the existence and direction of an amide bond upon the potential-driven dynamic behavior of adsorbed films of six different 4-pyridyl terminated surfactants in Scheme 1. The results may have great impacts on the understanding of potential-driven behavior and the rigidity of the compact adsorption films.

2. Experimental Section

2.1. Materials

Milli-Q water with resistivity of 18 MΩ cm was used to wash the glassware and to prepare all the aqueous solutions. Potassium perchlorate ($KClO_4$) was prepared by neutralizing $HClO_4$ (Ultrapure Analytical grade, Tama Chemicals) with KOH (Suprapure grade, Merck), collected by filtration, recrystallized twice from water, and dried in vacuum at 100 °C. Potassium bicarbonate ($KHCO_3$, reagent grade, Kanto Chemicals) and chloroform (spectral grade, Nakalai Tesque) were used as received. Wetted Ar gas (99.9995%) was used to deaerate the electrolyte solution.

N-Myristoyl-2-(4-pyridinyl)ethylamine (**C13-CONH-C2Py**) was synthesized as follows.

Myristoyl chloride (3.0 mmol) was added dropwise to the dry chloroform solution (50 ml) containing 4-(2-aminoethyl)pyridine (4.0 mmol) and triethylamine (3.0 mmol) under N_2 atmosphere at 0 °C. The solution was stirred for 1 h at 0 °C and then for 72 h at room temperature. The reaction solution was washed sequentially with 3 × 0.1 M HCl, 3 × 0.1 M $KHCO_3$, and 3 × brine. The organic phase was dried with $MgSO_4$, and the solvent was evaporated. The crude product as a white powder was recrystallized twice from acetone/water to yield the purified compound, which was analyzed by elemental analysis (EA), ^{1}H NMR and IR. m.p., 58.5 – 59.7 ºC

N-Tridecyl-*β*-(4-pyridyl)-propionamide (**C13-NHCO-C2Py**) was synthesized via the amide coupling of *β*-(4-pyridyl)-propionic acid and tridecylamine. *β*-(4-Pyridyl)-propionic acid was prepared from 4-(*γ*-hydroxypropyl)-pyridine following the reported procedure [46]. *β*-(4-Pyridyl)-propionic acid (3.4 mmol) was dissolved in 30 mL of dry dimethylacetamide (DMAc) under N_2 atmosphere. 1-Ethyl-3-(3-dimethylaminopropyl)-carbodiimide hydrochloride (5.0 mmol) was added to this solution at 0 °C. After the reaction solution was stirred for 1 h, tridecylamine (3.2 mmol) and triethylamine (5.0 mmol) were added at 0 °C. The solution was stirred for 1 h at 0 °C and for 72 h at room temperature. Water (300 mL) was added to the reaction mixture to obtain a suspension, which was then extracted with ethylacetate. Removal of the organic solvent gave orange oil presumably containing triethylamine and/or DMAc. The oil was recrystallized twice from acetone/water to yield white crystal, which was analyzed by EA, ^{1}H NMR, and IR. m.p., 64.6 – 65.4 ºC.

Pentadecyl 4-pyridyl ether (**C15-O-Py**) was synthesized via Mitsunobu reaction. 4-Hydroxypyridine (8.0 mmol), 1-pentadecanol (4.0 mmol), and triphenyl phosphine (8.0 mmol) were added to 15 mL of dry tetrahydrofuran (THF), which was pre-distilled from Na under N_2. Azodicarboxylic acid diethyl ester (8.0 mmol, 40% in toluene) was slowly added to the solution under stirring. After stirring for 48 h at room temperature, the solvent was removed to yield a sticky residue. The residue was extracted with hexane and the suspension was filtered. The crude product collected by solvent evaporation from the filtrate was recrystallized from acetone to yield white powder, which was analyzed by EA, ^{1}H NMR, and IR. m.p., 41.8 – 43.4 ºC.

1-Pyridin-4-yl-hexadecan-1-one (**C15-(C=O)-Py**) was synthesized as follows. After magnesium (8.0 mmol) was placed in a round-bottom flask, the apparatus was dried under

vacuum followed by N_2 flushing. Pre-distilled dry THF (10 mL) was added and 1-bromopentadecane (4.0 mmol) was slowly introduced under stirring. Stirring of the solution was continued until the flask was spontaneously cooled to room temperature. The reaction solution was added dropwise to another flask contained isonicotinonitrile (6.0 mmol) solution of dry THF (10 mL) with stirring under N_2. After stirred for 24 h at room temperature, the mixture was hydrolyzed with 10% hydrochloric acid solution. The THF in this solution was selectively removed by evaporation, and the obtained suspension was extracted with diethyl ether. The organic phase was washed with 3 × 0.1 M $KHCO_3$ and 3 × brine, dried with $MgSO_4$ and removed by evaporation. The crude product as a yellow sticky residue was dissolved in hexane and cooled to –20 °C. Precipitated white gel-like solid was collected by filtration and recrystallized from hexane to yield the purified compound. The product was analyzed by EA, ^{1}H NMR, and IR. m.p., 75.4 – 76.6 ºC.

A Au(111) of a single crystal disk (Techno Chemics Inc., facet precision < 1 º) with a surface area of 0.264 cm^2 was used as a working electrode. Before each experiment, it was flame-annealed and quenched with Milli-Q water. The quality of the Au(111) electrode was checked by recording the cyclic voltammogram (CV) and differential capacitance-potential (*C–E*) curve in 50 mM $KClO_4$ before each experiment with surfactants. The reference electrode was a Ag/AgCl/sat-KCl in a separate compartment connected to the electrochemical cell through a salt bridge. All potentials reported here are referenced to this Ag/AgCl/sat-KCl electrode. The counter electrode was a flame-annealed gold coil. Electrolyte solution was 50 mM $KClO_4$ + 2 mM $KHCO_3$.

2.2. Electrochemical measurements

All the glassware used was boiled in a 1:1 mixture of nitric and sulfuric acids, and rinsed copiously with water before use. The cell filled with electrolyte solution was deaerated with Ar. Wetted Ar gas was flowed over the top of the solution during electrochemical experiments. The working electrode, after annealed and quenched with water, was introduced into the cell under the protection of Au(111) surface with a water droplet and set in a hanging-meniscus (H-M) configuration. To check the quality of the Au(111) electrode and the cleanness of electrode-electrolyte interface, CV and *C–E* curves were measured in 50 mM

$KClO_4$ solution and subsequently 50 mM $KClO_4$ + 2 mM $KHCO_3$ solution. When these results were identical to well-known responses, experiments with surfactants were undertaken.

The deposition of the film to the electrode surface was performed using either single-touch or double-touch method. A portion of 1 mM surfactant solution in chloroform was spread onto the surface of aqueous electrolyte solution (gas/solution interface) until the surfactant solution formed meta-stable lenses at the interface for at least 30 s. In this condition, the surface pressure of Langmuir film of the surfactant reached the equilibrium spreading pressure. After 10 min, the pretreated clean working electrode was put in the cell under Ar to cool to room temperature. In the pretreatment, the electrode was flame-annealed, quenched with Milli-Q water, and flame-annealed again. The electrode after cooled was horizontally touched to the electrolyte surface at an open circuit condition to form a single-touch film of surfactants on the electrode surface and set in a H-M configuration. In the double-touch method, the electrode with a single-touch surfactant film was detached from the electrolyte solution. The remaining solution droplets on the electrode surface were removed using a capillary. The electrode was horizontally touched again to the surfactant-covered electrolyte solution surface to form a double-touch film.

A potentiostat (Toho Giken, Polarization Unit PS-06 with a 50 μs response time) and a digital lock-in-amplifier (EG&G Instruments, DSP 7265) were employed to control and measure the electrical variables of the interface. The differential capacitance (C) was measured by superimposing an ac perturbation of 5 mV_{rms} and 14 Hz on a 5 mV s^{-1} voltage ramp. In the calculation of C, a constant resistor-capacitor series equivalent circuit was assumed. Potential step sequence measurements were conducted by using a Huso Electro Chemical System (HUSO, HECS326-1 head box, response time 0.5 μs) to obtain a sequence of chronoamperograms. The current transients were numerically integrated to obtain the surface charge (σ_M)–E curves. The calculation procedure was the same as that in ref. 17. All the electrochemical measurements were conducted at room temperature (25 ± 1 ºC).

3. Results and discussion

3.1. Calculation of molecular structures and properties

Fig. 1 shows molecular structures optimized by MOPAC calculations for six different surfactants. Molecular properties, which most relevantly determine the behavior of the surfactant films on an electrode surface, may include excess electronic charge on the pyridyl nitrogen and the molecular dipole moment. These are added in Fig. 1 as the results of the MOPAC2000 conventional calculations with the AM1 Hamiltonian followed by EF geometrical optimization in vacuum. Note that molecular structures are drawn in the way that the dipole moments are presented on paper.

Fig. 1

The excess electronic charge on the pyridyl nitrogen for **C15-O-Py** and **C15-(C=O)-Py** are actually quite different as being predicted: **C15-O-Py** has much higher value (–0.164) than **C15-(C=O)-Py** (–0.119). **C13-CONH-C2Py** and **C13-NHCO-C2Py** have almost the same values of excess electronic charge (–0.139 and –0.137, respectively), being similar to that of **C15-Py** (–0.142).

To discuss the orientation of the surfactants on the electrode surfaces in the following sections, it is useful to divide the dipole moment into two orthogonal components. Namely, one is parallel to the C2 axis of pyridyl ring and the other is perpendicular to the plane of pyridyl ring. The dipole moments for **C15-O-Py** and **C15-(C=O)-Py** are positioned almost on the plane formed by the pyridyl ring. **C15-O-Py** has a large component parallel to the C2 axis and a small one perpendicular to the plane of pyridyl ring. In contrast, **C15-(C=O)-Py** has a small component parallel to the C2 axis and a large one perpendicular to the plane of pyridyl ring. In the case of **C13-CONH-C2Py** and **C13-NHCO-C2Py**, the dipole moments are not positioned on a plane formed by the pyridyl ring. The dipole moments for **C13-CONH-C2Py** and **C13-NHCO-C2Py** are tilted by 10 º and 16 º with respect to the plane of pyridyl ring, respectively. **C13-CONH-C2Py** has a larger component parallel to C2 axis compared to **C13-NHCO-C2Py**.

These optimized structure and dipole moments obtained by the MOPAC calculation are not necessarily illustrate the actual conformations of the surfactants in their compactly packed

films on the electrode surface. Nevertheless, Zamlynny found that the structure of **C15-Py** molecule in its compactly packed film on a Au(111) surface roughly resembles the expected geometrical structure [20]. Following discussions using dipole moments are based on the assumption that the structures of molecules in the compactly packed film are not far different from the structures obtained by MOPAC calculations.

3.2. Electrochemical measurements

We use the results of the measurements of CVs, *C*–*E* curves, and σ_M–*E* curves to describe the potential dependent structures of surfactant films. We found that all newly investigated surfactant molecules also desorb from the Au(111) electrode surface around –0.80 V and re-form compact films around 0.00 V. The details of their potential-driven phase change behavior were obviously varied depending on their molecular structures. For the single-touch film of a given surfactant, however, the results of electrochemical measurements showed also sample-to-sample variability, for example, in the potentials of adsorption/desorption and reorientation, peak heights, and minimum values of *C* in the *C*–*E* curves, although the trends of molecule dependence were quite clear. Most likely, single-touch film formation is not rigorously controllable so that the origin of the variability may be due to slight differences in defects in the monolayer and/or partial bilayer formation. Hence, the data shown for single-touch films in this paper should be considered as representatives of many experiments while accurately reflecting the general behavior. On the other hand, double-touch films showed high reproducibility in many experiments. Therefore, we evaluate the effects of the electronic property and amide group upon the potential-driven behavior mainly using the results of double-touch films. Note that the voltammetric data for single-touch films shown in this paper are for the sample that exhibited the highest minimum value of *C* in the *C*–*E* curve among those represented reproducible double-touch film data in subsequent examination for the same sample.

In the following subsections, we first discuss the effect of the excess charge of pyridyl nitrogen on the behavior. Then, we highlight the effect of the presence of the intermolecular hydrogen bonding between amide groups and the direction of amide bonds.

3.2.1. Influence of excess charge of pyridyl nitrogen

When **C15-Py** is adsorbed on a Au(111) electrode surface using the single-touch procedure, its 4-pyridyl head group is bound to the surface through the lone pair electrons of pyridyl nitrogen with ordered upright orientation of alkyl chains in the condensed film around the potential of zero charge (pzc) of a bare electrode [17,20]. It is likely that 4-pyridyl terminated surfactants other than **C15-Py** also adsorb with the 4-pyridyl head group down to the Au(111) surface around the pzc. Therefore, the excess charge of pyridyl nitrogen should be one of the key factors governing the potential dependent dynamic behavior in the whole potential region examined. Among the six surfactant molecules in Fig. 1, **C15-O-Py** has the highest value of the excess charge of pyridyl nitrogen, while **C15-(C=O)-Py** has the lowest.

The CVs and *C–E* curves for single-touch films of these two different surfactants are shown in Fig. 2. First, we are concerned with the response to the negative potential scan from 0.20 V. At this initial potential, these surfactants exhibited a low value of capacitance (ca. 7.0 μF cm^{-2}), indicative of compactly packed film formation of both surfactants on the electrode surface. **C15-O-Py** showed small capacitance peaks in the potential region –0.10 to –0.40 V (Fig. 2-B), most likely corresponding to the reorientation of its pyridyl group. On the other hand, **C15-(C=O)-Py** showed large and sharp reorientation peaks in the potential region 0.10 to –0.40 V (Fig. 2-D), corresponding to the transition to a loose film possessing a high capacitance value (13 μF cm^{-2}). The reorientation of **C15-(C=O)-Py** commenced at more positive potential than that of **C15-O-Py**. When moving the electrode potential further to negative, the capacitance for these two surfactants increased and reached almost the same value as the film-free electrode around –0.80 V, indicating that these two surfactants desorb from the electrode surface.

Fig. 2

When the direction of potential sweep was reversed at the negative end potential, the capacitance for **C15-O-Py** gradually decreased and reached a minimum value (5.5 μF cm^{-2}) around –0.05 V, indicating that a compact film are re-formed in this potential region. On the other hand, the capacitance for **C15-(C=O)-Py** gradually decreased followed by small and

very large peaks, respectively at –0.20 V and –0.05 V. At 0.15 V, the minimum value (7.5 μF cm^{-2}) as the same as at the initial state was restored. All peaks in CVs (Figs. 2-A and C) corresponded well to either peaks or steep slopes in the *C–E* curves. However, the CV peak positions were not always consistent with the capacitance peak positions. The cross relationship between CV and *C–E* curves will be discussed later in more detail.

Fig. 3 represents the CVs and *C–E* curves for double-touch films of **C15-O-Py** (A and B) and **C15-(C=O)-Py** (C and D). In the course of negative potential scan from 0.40 V, **C15-O-Py** showed no reorientation peak, while a gradual increase of capacitance was followed by its steep rise reaching the value of a bare Au(111) electrode around –0.80 V, at which the molecules desorbed from the electrode surface. In sharp contrast, **C15-(C=O)-Py** showed a reorientation peak of pyridyl group clearly around –0.28 V, and then, the film desorbed from the electrode surface at –0.80 V. In the reverse potential scan, the capacitance for **C15-O-Py** monotonically decreased through three stages, sharp drop between –0.70 V and –0.60 V, gradual decrease between –0.50 V and –0.30 V, and restoration of the minimum value of 1.0 μF cm^{-2} at 0.10 V. The first stage corresponds to the re-adsorption of surfactants onto the Au(111) surface, and the third stage does to the restoration of a compact film. As for **C15-(C=O)-Py**, the capacitance started decreasing around –0.55 V, exhibited a small peak corresponding to the reorientation of pyridyl group at –0.22 V, and finally reached a minimum value of 3.0 μF cm^{-2}. Most of the peak potentials in CVs agreed well with the potentials of either steep changes or peaks of capacitance in the *C–E* curves. However, the *C–E* curves did not show exact correspondence to the CVs. For example, the CV for **C15-O-Py** exhibited current humps in the potential region –0.50 V to –0.70 V on the negative-going scan and around 0.00 V in the positive-going scan, both being likely due to the phase transitions of the adsorbed film. In contrast, the *C–E* curves exhibited only subtle changes of capacitance in these potential regions. Also for the **C15-(C=O)-Py** double-touch film, the same phenomenon was observed around –0.40 V in the positive-going scan. Again, the cross relationship between CV and *C–E* curve will be discussed later.

Fig. 3

Fig. 4 shows the σ_M–*E* curves for double-touch films of **C15-O-Py** (A) and

C15-(C=O)-Py (B). Triangles and circles show, respectively, the desorption and adsorption processes. The curves for desorption process were obtained as follows. The electrode potential was first stepped from a constant potential of E_s to E_i, where $E_i = E_s - 0.02\ \mathrm{V} \times i$ (i = 1, 2, 3, ···). E_s was set at the potential at which a compact layer is formed. The values of E_s were fixed at 0.40 V for **C15-O-Py** and 0.22 V for **C15-(C=O)-Py**. After the step, new equilibrium state was established at E_i during an equilibration time period of 60 s. Then, the potential was stepped back to E_s to record a transient current. The charge needed to reach equilibrium at E_s is equivalent to the charge required for the desorption process by the step from E_s to E_i. The curves for adsorption process were measured in the same way as the desorption process, except for the potentials of E_s (E_s is –0.90 V for **C15-O-Py** and –0.82 V for **C15-(C=O)-Py**) and $E_i = E_s + 0.02\ \mathrm{V} \times i$. Note that, in the measurement of the adsorption process, the double-touch film of **C15-(C=O)-Py** was slightly destroyed by holding it at very negative potential and/or repetitive potential stepping to E_s. Namely, after the potential step measurements, adsorption peak around –0.57 V in CV was substantially diminished.

Fig. 4

In the desorption process of **C15-O-Py** (Fig. 4-A), σ_M showed almost a constant value in the range from E_s (0.40 V) down to –0.30 V. Two-stage decreases of σ_M around –0.40 V and –0.70 V followed. These decreases reflect, respectively, phase transition due to reorientation of 4-pyridyl groups and desorption processes. For **C15-(C=O)-Py** (Fig. 4-B), the decrease in σ_M due to the phase transition was observed around –0.25 V, and that due to desorption was observed around –0.65 V. In the adsorption process, an increase of σ_M relative to that of a bare electrode commenced around –0.75 V for **C15-O-Py** and –0.57 V for **C15-(C=O)-Py**. This increase is due to the adsorption of surfactant molecules. The second stage increases of σ_M due to the phase transition were observed in the potential range from –0.20 V to 0.00 V for **C15-O-Py** and from –0.30 V to –0.20 V for **C15-(C=O)-Py**.

Overall, changes of σ_M due to the phase transition and desorption/adsorption processes correlated well with the CVs. The correlation among CVs, C–E curves and σ_M–E curves, however, was incomplete, as described earlier. One of the reasons of the inconsistency is

related to the kinetics of potential dependent changes. The charge density (σ_M) is a function of coverage (Γ) and potential (E), and Γ is a function of E. Therefore, the differential capacitance (C) is described as

$$C = \frac{d\sigma_M}{dE} = \left(\frac{\partial \sigma_M}{\partial E}\right)_\Gamma + \left(\frac{\partial \sigma_M}{\partial \Gamma}\right)_E \frac{d\Gamma}{dE} \quad (1)$$

When being absent of kinetic retardation, frequency independent $d\Gamma/dE$ term directly determines the peaks in C–E curves. However, if the kinetics of the potential induced changes in Γ is slow, Eq. (1) may be written as

$$C = \frac{d\sigma_M}{dE} = \left(\frac{\partial \sigma_M}{\partial E}\right)_\Gamma + \left(\frac{\partial \sigma_M}{\partial \Gamma}\right)_E \frac{d\Gamma}{dt}\frac{dt}{dE} \quad (2)$$

If the kinetics is sufficiently slow with respect to the frequency, $d\Gamma/dt$ becomes zero and hence, $d\Gamma/dE = 0$. Then, featureless C–E curves are observed. The insensitivity of the capacitance changes while the changes of CV current may be attributed to the sluggish kinetics of the phase transitions.

Taken the results of CVs, C–E curves and σ_M–E curves together, remarkable differences of the behavior between **C15-O-Py** and **C15-(C=O)-Py** were found for both single- and double-touch films. The most noticeable difference is the sharpness and amplitude of the phase transitions around −0.2 V in the negative going scan. **C15-(C=O)-Py** film exhibited the distinct phase transition from condensed film to loose film in the negative going scan. For example, this reflects in the C–E curves as a large difference in capacitance values between before and after the phase transition. On the other hand, **C15-O-Py** film exhibited small or no changes in the value of capacitance around −0.2 V. This indicates that the reorientation of pyridyl groups in **C15-(C=O)-Py** films takes place more easily compared to **C15-O-Py** films. **C15-(C=O)-Py** possesses a lower excess electronic charge on its pyridyl nitrogen, leading to a weaker interaction with the Au surface when assuming an upright orientation, than **C15-O-Py**. Therefore, vertical orientation for **C15-(C=O)-Py** is less stable than that of **C15-O-Py**, facilitating the phase transition from a condensed to loose film. Note that the susceptibility to potential change also depends on the whole molecular

structures of the surfactants. Zamlynny and coworkers found in their polarization-modulation IR reflection spectra that the 4-pyridyl group as the head group of **C15-Py** exhibits a smaller amplitude of the tilt angle changes with potential than pyridine molecule [20]. This arises from both steric hindrance and lateral intermolecular interaction between alkyl chains. The differential capacitance of condensed film of **C15-(C=O)-Py** was relatively high compared to that of **C15-O-Py** (Figs. 2 and 3). This fact indicates that the molecular packing of **C15-(C=O)-Py** on the electrode surface is relatively loose and penetration of solvent molecules into the adsorbed films is allowed, provided that the dielectric constant and thickness of the condensed film produced by these surfactants are same if their molecular densities in the film are the same. Both loose packing and solvent penetration result in a weaker lateral interaction between adsorbed molecules. Consequently, the film of **C15-(C=O)-Py** adsorbed on the gold surface has lower rigidity than **C15-O-Py**, facilitating its reorientation.

Fig. 4 demonstrates that the σ_M for the two surfactant films were quite different in the compact film potential region (10 μC cm^{-2} for **C15-O-Py** and -8 μC cm^{-2} for **C15-(C=O)-Py**). The apparent pzc for these surfactants were also different. That for the **C15-O-Py** covered electrode was far more negative than that of a bare Au(111) electrode, whereas that for **C15-(C=O)-Py** was more positive. For an electrode covered by a film, the shift of the pzc relative to that of a bare Au(111) could be described by the Helmholtz formula:

$$\Delta E_{\mathrm{pzc}} = \Gamma(\mu_{\perp}^{org} - n\mu_{\perp}^{water}) / \varepsilon \qquad (3)$$

Where Γ is the superficial concentration of the surfactant molecules, $\mu_{\perp}^{org}$ and $\mu_{\perp}^{water}$ are the components of the dipole moments in the direction normal to the surface, superscripts "org" and "water" stand for the organic and water molecules, n is the number of water dipoles replaced by one adsorbed surfactant molecule at the electrode surface, and ε is the dielectric permittivity of the inner layer. In the case of **C15-O-Py**, since the shift of pzc is to largely negative, its dipole moment is highly aligned with a direction down to the electrode surface in the condensed film region (i.e., around 0.20 V), compared with water-covered electrode. On the other hand, since the shift of pzc for **C15-(C=O)-Py** is positive, its dipole moments appear

to direct toward electrolyte solution. This difference of dipole orientation probably results from the difference of direction of dipole moment with respect to the pyridine ring and compactness of adsorbed film. The dipole moment of **C15-O-Py** has a dominant component parallel to the C_2 axis of the pyridyl group (Fig. 1). When the pyridyl group assumes an upright orientation, the dipole moment of **C15-O-Py** almost directs to the surface. Therefore, it is reasonable that the surface charge for the gold surface covered by **C15-O-Py** exhibits the positive value in the compact film region. On the other hand, **C15-(C=O)-Py** has a small component parallel to the C_2 axis directed to nitrogen of pyridyl group (Fig. 1). This component has only a minor contribution to the surface charge when the pyridyl group assumes upright orientation. A slight tilting and/or twisting of the molecule could result in even a negative contribution. Furthermore, because the packing density of **C15-(C=O)-Py** is relatively low, the dipole moment of solvents, if being penetrating, also contributes to the surface charge of the Au(111) surface. As a result, the electrode surface covered by **C15-(C=O)-Py** may exhibit a negative value of σ_M around 0.1 V.

It is worthwhile to compare the behavior of **C15-O-Py** and **C15-(C=O)-Py** to that of **C15-Py** [18]. The value of electronic excess charge of pyridyl nitrogen of **C15-Py** is –0.142, which is about an intermediate value of other two. The *C–E* curves for single-touch and double-touch films of **C15-Py** reported in ref. 18 are quoted and shown as insets, respectively, in Fig. 2-B and Fig. 3-B. Minimum values of capacitance of both single- and double-touch films of **C15-Py** were comparable to those of **C15-O-Py** but lower than those of **C15-(C=O)-Py**. The *C–E* curve for the **C15-Py** double-touch film did not show any reorientation peak in the negative potential scan, being similar to the behavior of **C15-O-Py** but different from the behavior of **C15-(C=O)-Py**. The origin of this marked difference of *C–E* curve between **C15-Py** and **C15-(C=O)-Py** is the difference of either or both the strength of lateral intermolecular interaction and the electronic charge of the pyridyl nitrogen. Both the double-touch films of **C15-Py** and **C15-O-Py** had almost the same minimum value of capacitance (1 $\mu F\ cm^{-2}$), suggesting that these adsorbed films have almost the same compactness. However, the onset potential of the desorption for the **C15-Py** double-touch film, represented by a rapid increase of the differential capacitance at about –0.65 V (Fig. 3-B), was less negative than that of the desorption for **C15-O-Py** (–0.77 V). This onset potential difference may be due to the difference of the excess charge of pyridyl nitrogen but

not to the difference of strength of the lateral intermolecular interaction.

3.2.2. Effect of the presence and direction of amide group

The excess charge of pyridyl nitrogen for both **C13-CONH-C2Py** and **C13-NHCO-C2Py** are almost equivalent to that of **C15-Py**. Therefore, comparison of the behavior among these three surfactants may allow for the evaluation of the effects of the presence and direction of amide group upon the potential-driven phase change. Fig. 5 shows the CVs and *C–E* curves for single-touch films of **C13-CONH-C2Py** (A and B) and **C13-NHCO-C2Py** (C and D). Fig. 6 shows those for the double-touch films.

Fig. 5

Fig. 6

The *C–E* curves of single-touch films (Fig. 5-B and D) showed a steep rise of capacitance at positive potentials. At a bare Au(111) electrode surface, adsorption of bicarbonate ion occurs in this potential region [47]. Therefore, the capacitance rise gives evidence of the penetration of bicarbonate ion into the adsorbed films. Both surfactants of interest exhibited a minimum value of *C* of ca. 7.0 μF cm^{-2} around –0.10 V. This higher value than that of **C15-Py** single-touch film (Fig. 2-B) implies the reduction of the molecular packing by the introduction of the amide group. When the electrode potential was moved in the negative direction, the capacitance for **C13-CONH-C2Py** gradually increased at potentials lower than –0.28 V, and reached the value near to the film-free electrode at –0.80 V at which desorption of the molecules from the electrode surface largely took place. However, the desorption was incomplete, since the value of capacitance at –0.80 V was still slightly lower than that for the film-free electrode. As for **C13-NHCO-C2Py**, small and broad capacitance peaks were observed at 0.00 V and –0.30 V. The capacitance gradually increased at the further negative potentials. Around –0.80 V, the capacitance was higher than that of a film-free electrode, most likely due to simultaneous occurrence of hydrogen evolution. In the course of positive potential scan, the capacitance for **C13-CONH-C2Py** started a gradual decrease around –0.75 V, sharply decreased around –0.45 V, and then

reached a minimum value of ca. 8.0 μF cm^{-2}. The capacitance of **C13-NHCO-C2Py** immediately dropped when the direction of potential sweep was reversed and then gradually decreased and reached a minimum value of 7.0 μF cm^{-2}. Peaks and shapes of CVs for these compounds were in good agreement with the changes of capacitance and peaks of corresponding *C–E* curves. In **C13-NHCO-C2Py**, both desorption and readsorption peaks were not clearly observed in CV. A small readsorption peak was observed when the electrode potential was swept further negative to –0.87 V, although desorption peak was obscured by the significant hydrogen evolution current. Note that the *C–E* curves in Fig. 5 were rather featureless compared to **C15-Py**, which exhibits an enhanced capacitance peak at –0.20 V due to the reorientation of its pyridyl group. The presence of an amide group in the midway of an alkyl chain either suppresses sharp reorientation of pyridyl group or interrupts the condensed film formation in the positive potential region. This is in line with the reports claiming that the existence of amide group perturbs the packing of alkyl chains [39,40,44].

For the double-touch films (Fig. 6), the capacitance minimum was 3.0 μF cm^{-2} for **C13-CONH-C2Py** (Fig. 6-A) and 1.8 μF cm^{-2} for **C13-NHCO-C2Py** (Fig. 6-B). In the negative potential scan, **C13-CONH-C2Py** showed no reorientation peak, and the capacitance was almost constant down to –0.55 V. Then, the capacitance gradually increased in more negative potential region and finally reached a value near to that for a bare Au(111) electrode around –0.87 V. In the case of **C13-NHCO-C2Py**, the capacitance increased slightly around –0.30 V, corresponding to the reorientation of its pyridyl group, and steeply around –0.55 V, and exceeded the value for a bare Au(111) electrode around –0.87 V. When the electrode potential was scanned to positive, the capacitance for **C13-CONH-C2Py** decreased from –0.70 V and reached a plateau region (ca. 4.4 μF cm^{-2}) around –0.30 V and subsequently decreased to be 3.9 μF cm^{-2} around 0.10 V. On the other hand, the capacitance for **C13-NHCO-C2Py** immediately decreased from –0.85 V, and a broad peak was obviously observed at –0.13 V. The capacitance reached a minimum value of 1.8 μF cm^{-2} at 0.30 V.

The minimum values of capacitance for these amide-containing surfactants were higher than that of **C15-Py** (1.0 μF cm^{-2}). This fact indicates that these amide-containing surfactants form more loosely packed films than **C15-Py**. The high minimum value for **C13-CONH-C2Py** suggests that this surfactant does not form a condensed film through phase transition even in the positive potential region. **C13-NHCO-C2Py** has the relatively lower

value of minimum capacitance compared to **C13-CONH-C2Py**, indicating the formation of more compact film than that of **C13-CONH-C2Py**. The double-touch film of **C13-NHCO-C2Py** shows the phase transition from compactly packed film to loosely packed film in the negative-going scan. In contrast, the double-touch film of **C15-Py** does not exhibit the changes of capacitance corresponding to reorientation in negative potential scan (Fig. 3-B inset). These results suggest that the double-touch films possessing amide group transform more easily from a compact film into a disordered film compared to amide free **C15-Py**. Furthermore, both double-touch films of **C13-CONH-C2Py** and **C13-NHCO-C2Py** exhibited a steep increase of capacitance from less negative potential (−0.55 V) compared to **C15-Py** (−0.65 V) in the negative potential scan. Taken together, the existence of amide group in the present case lowers the rigidity of the adsorbed film, facilitating the potential dependent phase change.

Above-mentioned effect of the existence of amide group appears inconsistent with most of the previous reports on amide-containing alkanethiol SAMs. Those reports concluded that the existence of amide group in the alkyl chain of the molecules increases the stability of the structure of the SAM [41,43,44]. Valiokas and coworkers reported that the temperature of thermal disordering of alkyl chain of a SAM of ω-hydroxy-alkyl thiol in ultrahigh vacuum was made much higher by introducing an amide group in its alkyl chain [42].

Most probable reason for this inconsistency is the presence of solvent water in our systems in contrast to the experiments in refs. 41-44. The existence of amide group allows for the penetration of water molecules into the adsorbed films in an aqueous solution due to loose packing of the alkyl chain and the high hydrophilicity of the amide group [40]. Water molecules in the film interior may be capable of hydrogen bonding formation with the amide group of the surfactants and reduce the density of alkyl chains of the film. As a result, the hydrogen bonding between amide groups and van der Waals interaction between alkyl chains are weakened, leading to a decrease in rigidity of the close-packed 4-pyridyl surfactant film. Indeed, Ong and coworkers found that the alkyl chain packing of 16-methoxyhexadecanethiol SAM is considerably disturbed by water molecules through the hydrogen bonding between ether group and water [48].

An exceptional case was reported by Sabapathy and coworkers so that stabilization of SAMs occurs due to the introduction of amide group even in an aqueous solution [49]. The

SAMs used by the authors are based on short alkanethiols with a bulky ferrocenyl group at their terminals. These ferrocenylalkylthiols originally do not form a closely packed film. In such a case, it is likely that the existence of amide bond does not substantially disturb the packing of alkyl chains. Therefore, the stabilization effect of hydrogen bonding between amid bonds works dominantly.

Actually, we also found a case that stabilization due to the existence of amide bond clearly appears. It is highlighted by the comparison of the potential dependent behavior between *N*-pentadecyl-4-pyridinecarboxamide (**C15-NHCO-Py**) and **C15-(C=O)-Py**. The excess charges of 4-pyridyl nitrogen of these surfactants are almost the same (Fig. 1). Thus, these two surfactants may have the same strength of attractive interaction with the gold surface when these pyridyl groups assume the vertical orientation. As described in 3.2.1, **C15-(C=O)-Py** does not form a close packed film in the compact film potential region. Therefore, in this comparison, the disturbance effect on alkyl chain packing due to the existence of amide bond may be small.

The *C*-*E* and σ_M–*E* curves for the double-touch film of **C15-NHCO-Py** are shown in Fig. 7. In the σ_M–*E* curve, only the desorption process are presented. The σ_M–*E* curve for desorption process of **C15-(C=O)-Py** (triangle) is superimposed to facilitate the comparison with **C15-NHCO-Py**. Because the behavior of **C15-NHCO-Py** double touch films was described in detail in our previous report [45], we briefly describe herein its behavior relevant to the comparison with **C15-(C=O)-Py**. (Note that the σ_M–*E* curve for **C15-NHCO-Py** in this report looks different from that in our previous report [45], because a different potential step procedure was used.)

Based on *C*-*E* curves (Fig. 3-D and 7-A), the films of these two surfactants have nearly the same compactness in the condensed film region as indicated by almost the same minimum value of capacitance (3.0 μF cm^{-2}). This suggests that, in this comparison, the introduction of amide bond does not affect the packing and interaction between alkyl chains. However, their potential dependent behaviors are clearly different. Particularly, in the desorption process, **C15-(C=O)-Py** film showed steep changes of *C* and σ_M around −0.25 V, indicating the sharp phase transition from the condensed film to loose film in the course of negative potential scan. On the other hand, **C15-NHCO-Py** film showed dull changes of *C* and σ_M around this potential, indicative of gradual phase transition. This difference suggests that the

existence of an amide group suppresses the reorientation of pyridyl group. In this comparison, the introduction of amide bond does not substantially disturb the packing. Therefore, destabilization effect due to the existence of amide bond does not clearly appear. Instead, the stabilization effect due to intermolecular hydrogen bonding between amid groups exclusively appears, resulting in suppressing reorientation of pyridyl group.

Fig. 7

Finally, we summarize the effect of direction of amide bond on the potential dependent behavior and the molecular assembling structures using **C13-CONH-C2Py** and **C13-NHCO-C2Py**. The single-touch film of **C13-NHCO-C2Py** was transformed, in the negative-going scan, from a closely packed film into a loosely packed film at the more negative potential than the film of **C13-CONH-C2Py**. The double-touch film of **C13-NHCO-C2Py** forms a closer packed film on the electrode surface in the positive potentials than **C13-CONH-C2Py**. The origin of these differences due to the difference of the amide direction, however, is unclear at this moment. Vollhardt and Wagner investigated the influence of the direction of amide bond introduced into the surfactants on the properties of the films formed at an air/water interface [50]. They found that the difference of amide bond direction causes the differences in the lattice structure of alkyl chains, the area occupied by one molecule, crystallinity, and morphology of condensed phase domain. This connotes that the direction of amide bond affects not only dipole orientation but also molecular assembling structure on an electrode surface. In our future work, we need to measure the potential dependent structures of the films in more detail in order for the roles played by amide groups to be fully clarified.

4. Conclusion

The major factors determining the potential-driven phase changes of the films of water-insoluble surfactants possessing a 4-pyridyl terminal group on a Au(111) electrode were investigated. By the use of six different surfactants, the results of electrochemical

measurements were used to elucidate the effects of electronic property of the 4-pyridyl group as the adsorption functional group and the existence of amide group in the alkyl chain upon their phase changes.

It is found that the surfactant possessing higher electronic excess charge on its pyridyl nitrogen tends to form a closer-packed film with upright orientation of the pyridyl group over a wider potential range. Typical of such a molecule is **C15-O-Py. C15-(C=O)-Py**, possessing the lowest electronic excess charge on the pyridyl nitrogen among the six molecules, is opposite in its behavior. The latter clearly exhibits potential-driven sharp reorientation of pyridyl group, while the former does not. The electronic property of the pyridyl group determines the strength of its attractive interaction with the electrode surface.

The effect of the existence and direction of amide bond in the alkyl chain of a surfactant on the potential-driven behavior is found to be of bilateral character. The net effect of the introduction of amide group upon the structure and behavior of the adsorbed film is determined by the balance between the ability of the amide group to disturb the alkyl chain packing and ability to increase film rigidity by hydrogen bonding network formation. In the case of a closely packed film, the existence of amide group lowers rigidity of the adsorbed film and facilitates the potential-driven phase transition from a condensed film to a loosely packed state. The existence of amide group helps the penetration of water molecules into the film interior, resulting in the disturbance of the alkyl chain packing. In sharp contrast, in the case of a loosely packed film, the existence of amide group suppresses the potential-driven phase transition. In this case, the existence of amide group increases the rigidity of the adsorbed film through intermolecular hydrogen bonding while hardly affects alkyl chain packing.

The present study has explicitly pointed out the importance of both molecule-surface and intermolecular interaction as major factors determining potential-driven phase changes of surfactant ultra-thin films on an electrode surface. These results may be indispensable when designing potential-controllable organic thin films. To shed light in more depth into the details of potential-dependent film structural changes and hydrogen bonding structures at a molecular level, we are currently undertaking in situ IR reflection measurements.

Acknowledgements

This work was financially supported in part by a Grant-in-Aids for Scientific Research B (no. 16350077 to T.S.). A financial support from Yazaki Memorial Foundation for Science and Technology to T.S. is also acknowledged.

References

[1] D. Bizzotto, V. Zamlynny, I. Burgess, C.A. Jeffrey, H.-Q. Li, J. Rubinstein, R.A. Merril, J. Lipkowski, Z. Galus, A. Nelson, B. Pettinger, in: A. Wieckowski (Ed.), Interfacial Electrochemistry: Theory, Experiment, and Applications, Marcel Dekker, New York, 1999, p. 405.

[2] I. Burgess, C.A. Jeffrey, X. Cai, G. Szymanski, Z. Galus, J. Lipkowski, Langmuir 15 (1999) 2607.

[3] Z. Tang, E. Wang, J. Electroanal. Chem. 496 (2001) 82.

[4] I. Burgess, V. Zamlynny, G. Szymanski, J. Lipkowski, Langmuir 17 (2001) 3355.

[5] J.J. Noel, D. Bizzotto, J. Lipkowski, J. Electroanal. Chem. 344 (1993) 343.

[6] D. Bizzotto, J.J. Noel, J. Lipkowski, Thin Solid Films 248 (1994) 69.

[7] D. Bizzotto, J. Lipkowski, J. Electroanal. Chem. 409 (1996) 33.

[8] D. Bizzotto, J.J. Noel, J. Lipkowski, J. Electroanal. Chem. 369 (1994) 259.

[9] D. Bizzotto, B. Pettinger, Langmuir 15 (1999) 8309.

[10] Y. Yang, D. Bizzotto, J. Electroanal. Chem. 500 (2001) 408.

[11] J. Shepherd, Y. Yang, D. Bizzotto, J. Electroanal. Chem. 524-525 (2002) 54.

[12] J.L. Shepherd, D. Bizzotto, J. Phys. Chem. B 107 (2003) 8524

[13] I. Zawisza, I. Burgess, G. Szymanski, J. Lipkowski, J. Majewski, S. Satija, Electrochim. Acta 49 (2004) 3651.

[14] I. Zawisza, J. Lipkowski, Langmuir 20 (2004) 4579.

[15] J.L. Shepherd, D. Bizzotto, Langmuir 22 (2006) 4869.

[16] D. Bizzotto, A. McAlees, J. Lipkowski, R. McCrindle, Langmuir 11 (1995) 3243.

[17] T. Sagara, V. Zamlynny, D. Bizzotto, A. McAlees, R. McCrindle, J. Lipkowski, Isr. J.

Chem. 37 (1997) 197.

[18] V. Zamlynny, I. Burgess, G. Szymanski, J. Lipkowski, J. Majewski, G. Smith, S. Satija, R. Ivkov, Langmuir 16 (2000) 9861.

[19] I. Burgess, V. Zamlynny, G. Szymanski, A.L. Schwan, R.J. Faragher, J. Lipkowski, J. Majewski, S. Satija, J. Electroanal. Chem. 550-551 (2003) 187.

[20] V. Zamlynny, I. Zawisza, J. Lipkowski, Langmuir 19 (2003) 132.

[21] A. Nelson, N. Auffret, J. Electroanal. Chem. 244 (1988) 99.

[22] D. Bizzotto, A. Nelson, Langmuir 14 (1998) 6269.

[23] V. Stauffer, R. Stoodley, J.O. Agak, D. Bizzotto, J. Electroanal. Chem. 516 (2001) 73.

[24] S.L. Horswell, V. Zamlynny, H.-Q. Li, A.R. Merrill, J. Lipkowski, Faraday Discuss. 121 (2002) 405

[25] R. Stoodley, D. Bizzotto, Analyst 128 (2003) 552.

[26] J.O. Agak, R. Stoodley, U. Retter, D. Bizzotto, J. Electroanal. Chem. 562 (2004) 135.

[27] S. Xu, G. Szymanski, J. Lipkowski, J. Am. Chem. Soc. 126 (2004) 12276.

[28] I. Burgess, M. Li, S.L. Horswell, G. Szymanski, J. Lipkowski, J. Majewski, S. Satija, Biophys. J. 86 (2004) 1763

[29] I. Burgess, M. Li, S.L. Horswell, G. Szymanski, J. Lipkowski, S. Satija, J. Majewski, Colloids Surf., B 40 (2005) 117

[30] D. Bizzotto, J.L. Shepherd, in: R.C. Alkire, D.M. Kolb, J. Lipkowski, P.N. Ross (Eds.), Diffraction and Spectroscopic Methods in Electrochemistry, WILEY-VCH, Weinheim, 2006, p. 97.

[31] V. Zamlynny, J. Lipkowski, in: R.C. Alkire, D.M. Kolb, J. Lipkowski, P.N. Ross (Eds.), Diffraction and Spectroscopic Methods in Electrochemistry, WILEY-VCH, Weinheim, 2006, p. 315.

[32] L. Stolberg, S. Morin, J. Lipkowski, D.E. Irish, J. Electroanal. Chem. 307 (1991) 241.

[33] J. Lipkowski, L. Stolberg, in: J. Lipkowski, P.N. Ross (Eds), Adsorption of Molecules at Metal Electrodes, VCH, New York, 1992, p. 201.

[34] J. Lipkowski, L. Stolberg, D.-F. Yang, B. Pettinger, S. Mirwald, F. Henglein, D.M. Kolb, Electrochim. Acta 39 (1994) 1045.

[35] W.-B. Cai, L.-J. Wan, H. Noda, Y. Hibino, K. Ataka, M. Osawa, Langmuir 14 (1998) 6992.

[36] M. Hoon-Khosla, W.R. Fawcett, A. Chen, J. Lipkowski, B. Pettinger, Electrochim. Acta 45 (1999) 611.

[37] B. Pettinger, J. Lipkowski, M. Hoon-Khosla, J. Electroanal. Chem. 500 (2001) 471.

[38] D.Y. Wu, M. Hayashi, C.H. Chang, K.K. Liang, S.H. Lin, J. Chem. Phys. 118 (2003) 4073.

[39] R.S. Clegg, J.E. Hutchison, Langmuir 12 (1996) 5239.

[40] R.S. Clegg, J.E. Hutchison, J. Am. Chem. Soc. 121 (1999) 5319.

[41] R.S. Clegg, S.M. Reed, J.E. Hutchison, J. Am. Chem. Soc. 120 (1998) 2486.

[42] R. Valiokas, M. Ostblom, S. Svedhem, S.C.T. Svensson, B. Liedberg, J. Phys. Chem. B 106 (2002) 10401.

[43] P.A. Lewis, R.K. Smith, K.F. Kelly, L.A. Bumm, S.M. Reed, R.S. Clegg, J.D. Gunderson, J.E. Hutchison, P.S. Weiss, J. Phys. Chem. B 105 (2001) 10630.

[44] S.-W. Tam-Chang, H.A. Biebuyck, G.M. Whitesides, N. Jeon, R.G. Nuzzo, Langmuir 11 (1995) 4371.

[45] T. Sagara, K. Uematsu, K. Nagata, J. Electroanal. Chem. 550-551 (2003) 219.

[46] F.H. McMillan, K.A. Kun, C.B. McMillan, J.A. King, J. Am. Chem. Soc. 78 (1956) 4077.

[47] K. Arihara, F. Kitamura, T. Ohsaka, K. Tokuda, J. Electroanal. Chem. 510 (2001) 128.

[48] T.H. Ong, R.N. Ward, P.B. Davies, J. Am. Chem. Soc. 114 (1992) 6243.

[49] R.C. Sabapathy, S. Bhattacharrya, M.C. Leavy, W.E. Cleland, Jr., C.L. Hussey, Langmuir 14 (1998) 124.

[50] D. Vollhardt, R. Wagner, J. Phys. Chem. B 110 (2006) 14881.

Legends for scheme and figures

Scheme 1. Molecular structures of **C15-O-Py**, **C15-(C=O)-Py**, **C13-CONH-C2Py** and **C13-NHCO-C2Py**. Structure of **C15-Py** and **C15-NHCO-Py** also are shown.

Fig. 1. Optimized structures of **C15-O-Py**, **C15-(C=O)-Py**, **C13-CONH-C2Py** **C13-NHCO-C2Py**, **C15-NHCO-Py** and **C15-Py** obtained by MOPAC2000 conventional calculation with the AM1 Hamiltonian followed by EF geometrical optimization in vacuum. Italic numbers represent the excess electronic charge on the pyridyl nitrogen atom, and arrows represent the dipole moments of the molecules.

Fig. 2. CVs (upper) and interfacial differential capacitance (*C*)–potential (*E*) curves (lower) for single-touch films of **C15-O-Py** (left, A and B) and **C15-(C=O)-Py** (right, C and D) in 50 mM $KClO_4$ + 2 mM $KHCO_3$ solution. The initial potential of CV was 0.00 V, and the sweep rate was 20 mV s^{-1}. *C–E* curves were obtained from ac voltammetric data measured at a frequency of 14 Hz, an ac amplitude of 5 mV_{rms}, and a dc potential sweep rate of 5 mV s^{-1} with the initial potential at the positive end of the curve (0.20 V). The dashed line represent the *C–E* curve for a bare Au(111) electrode. Inset figure in Fig. 2-B represent *C–E* curve for a single-touch film of **C15-Py** in 50 mM $KClO_4$ + 1 mM $KHCO_3$ solution reprinted with permission from ref. 18. Copyright (2000) American Chemical Society. The reference potential was converted to Ag/AgCl/sat-KCl from the original one (SCE).

Fig. 3. CVs (upper) and *C–E* curves (lower) for double-touch films of **C15-O-Py** (left, A and B) and **C15-(C=O)-Py** (right, C and D) in 50 mM $KClO_4$ + 2 mM $KHCO_3$ solution. Measurement conditions were the same as those in Fig. 2 except for the initial potentials of the potential sweep in *C–E* curves. Inset figure in Fig. 3-B represent *C–E* curve for a double-touch film of **C15-Py** in 50 mM $KClO_4$ + 1 mM $KHCO_3$ solution reprinted with permission from ref. 18. Copyright (2000) American Chemical Society. The reference potential was converted to Ag/AgCl/sat-KCl from the original one (SCE).

Fig. 4. Surface charge (σ_M)–*E* curves obtained from potential step sequence experiments for

double-touch films for **C15-O-Py** (A) and **C15-(C=O)-Py** (B). Open triangles, desorption process; open circle, adsorption process; dashed line, bare Au(111) electrode. In desorption processes, the electrode potential was first stepped from a constant potential of E_s to E_i ($E_i < E_s$), where $E_i = E_s - 0.02\ \mathrm{V} \times i$ (i = 1, 2, 3, ···). E_s was set at the potential at which a compact layer is formed (0.40 V for **C15-O-Py** and 0.22 V for **C15-(C=O)-Py)**. After the step, new equilibrium state was established at E_i during an equilibration time period of 60 s. Then, the potential was stepped back to E_s to record a transient current. The adsorption process were measured in the same way as the desorption process, except for the potential of E_s (E_s is –0.90 V for **C15-O-Py** and –0.82 V for **C15-(C=O)-Py**) and $E_i = E_s + 0.02\ \mathrm{V} \times i$. The calculation procedures were the same as ref. 17.

Fig. 5. CVs (upper) and *C*–*E* curves (lower) for single-touch films of **C13-CONH-C2Py** (left, A and B) and **C13-NHCO-C2Py** (right, C and D) in 50 mM $KClO_4$ + 2 mM $KHCO_3$ solution. Measurement conditions were the same as those in Fig. 2 except for the initial potentials of the potential sweep in *C*–*E* curves (0.40 V).

Fig. 6. CVs (upper) and *C*–*E* curves (lower) for double-touch films of **C13-CONH-C2Py** (left, A and B) and **C13-NHCO-C2Py** (right, C and D) in 50 mM $KClO_4$ + 2 mM $KHCO_3$ solution. Measurement conditions were the same as those in Fig. 2 except for the initial potentials of the potential sweep in *C*–*E* curves (0.40 V).

Fig. 7. *C*–*E* (A) and σ_M–*E* (B, squares) curves for double-touch film of **C15-NHCO-Py** in 50 mM $KClO_4$ + 2 mM $KHCO_3$ solution. In part B, a σ_M–*E* curve for a **C15-(C=O)-Py** double-touch film is added using triangles. Both σ_M–*E* curves shows desorption processes.

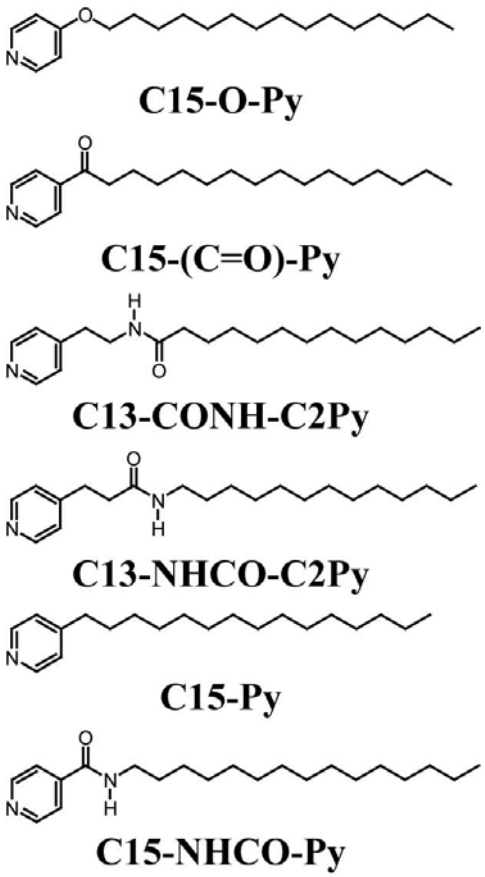

Scheme 1.

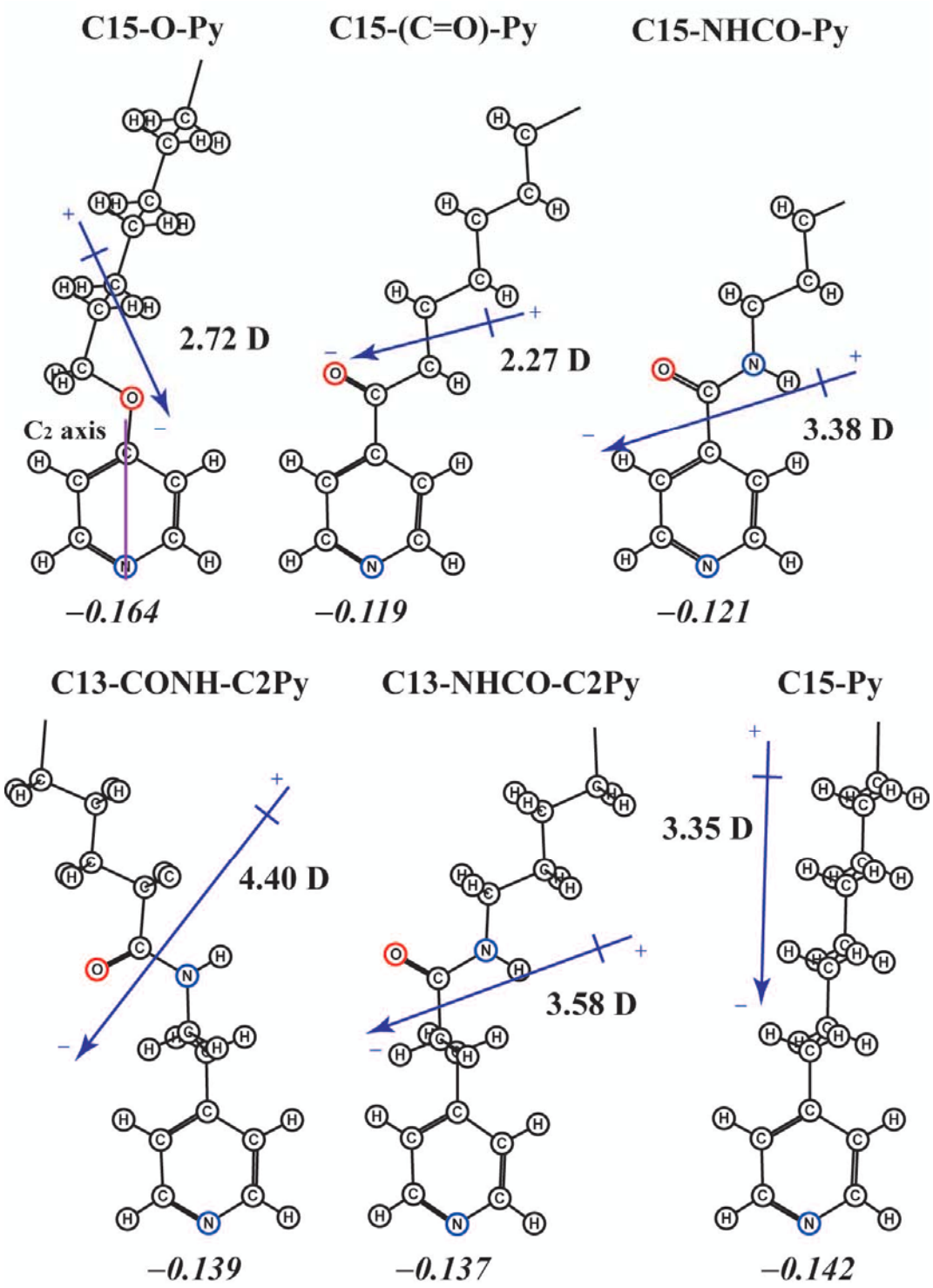
C15-O-Py
C15-(C=O)-Py
C15-NHCO-Py
2.72 D
2.27 D
3.38 D
C2 axis
−0.164
−0.119
−0.121
C13-CONH-C2Py
C13-NHCO-C2Py
C15-Py
4.40 D
3.58 D
3.35 D
−0.139
−0.137
−0.142

Fig. 1.

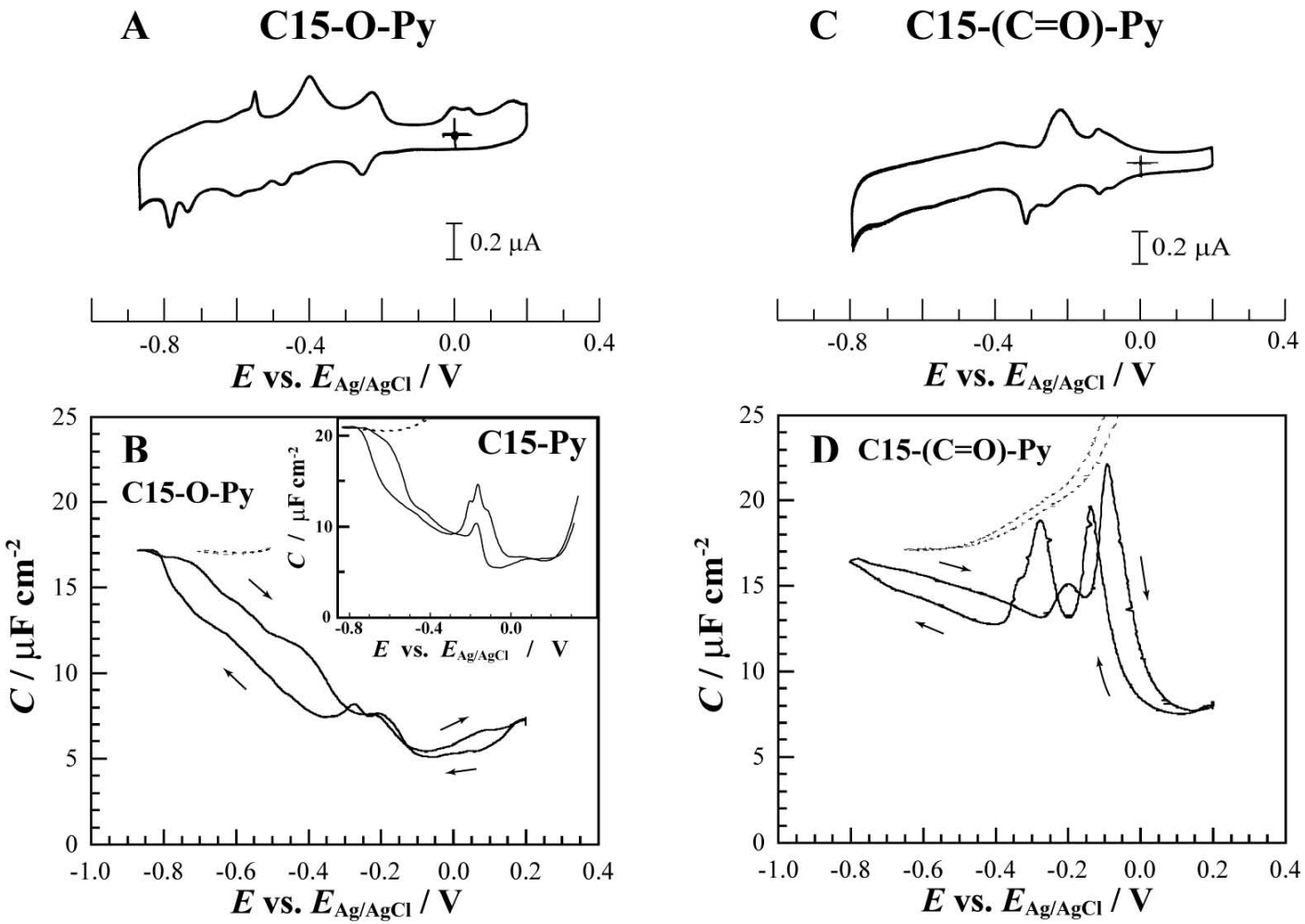
A
C15-O-Py
0.2 μA
-0.8
-0.4
0.0
0.4
E vs. E Ag/AgCl / V
C
C15-(C=O)-Py
0.2 μA
-0.8
-0.4
0.0
0.4
E vs. E Ag/AgCl / V
B
C15-O-Py
C15-Py
C / μF cm-2
E vs. E Ag/AgCl / V
D C15-(C=O)-Py
C / μF cm-2
E vs. E Ag/AgCl / V

Fig. 2.

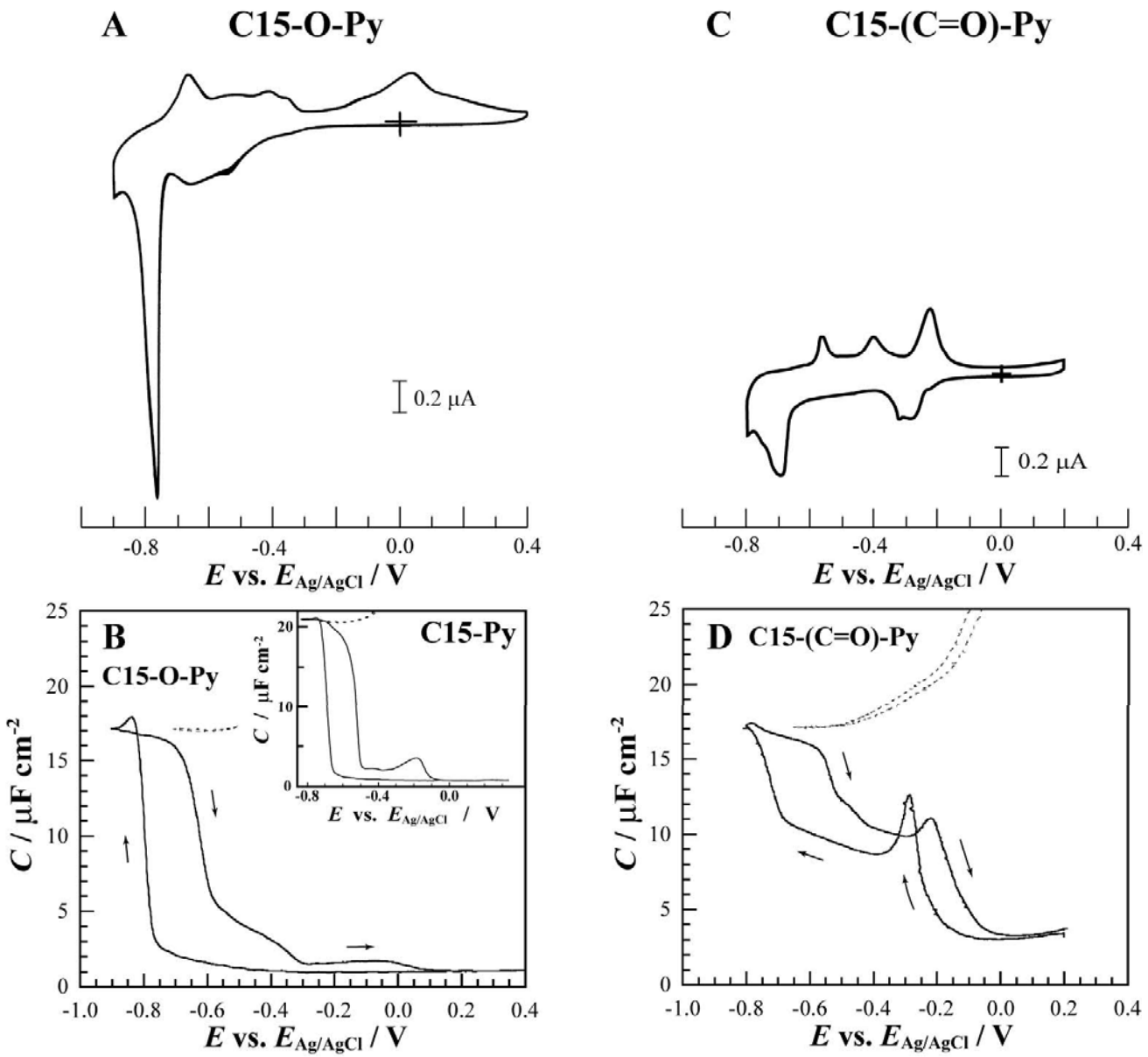
A
C15-O-Py
0.2 μA
-0.8
-0.4
0.0
0.4
E vs. E Ag/AgCl / V
C
C15-(C=O)-Py
0.2 μA
-0.8
-0.4
0.0
0.4
E vs. E Ag/AgCl / V
B
C15-O-Py
C15-Py
C / μF cm-2
E vs. E Ag/AgCl / V
D C15-(C=O)-Py
C / μF cm-2
E vs. E Ag/AgCl / V

Fig. 3.

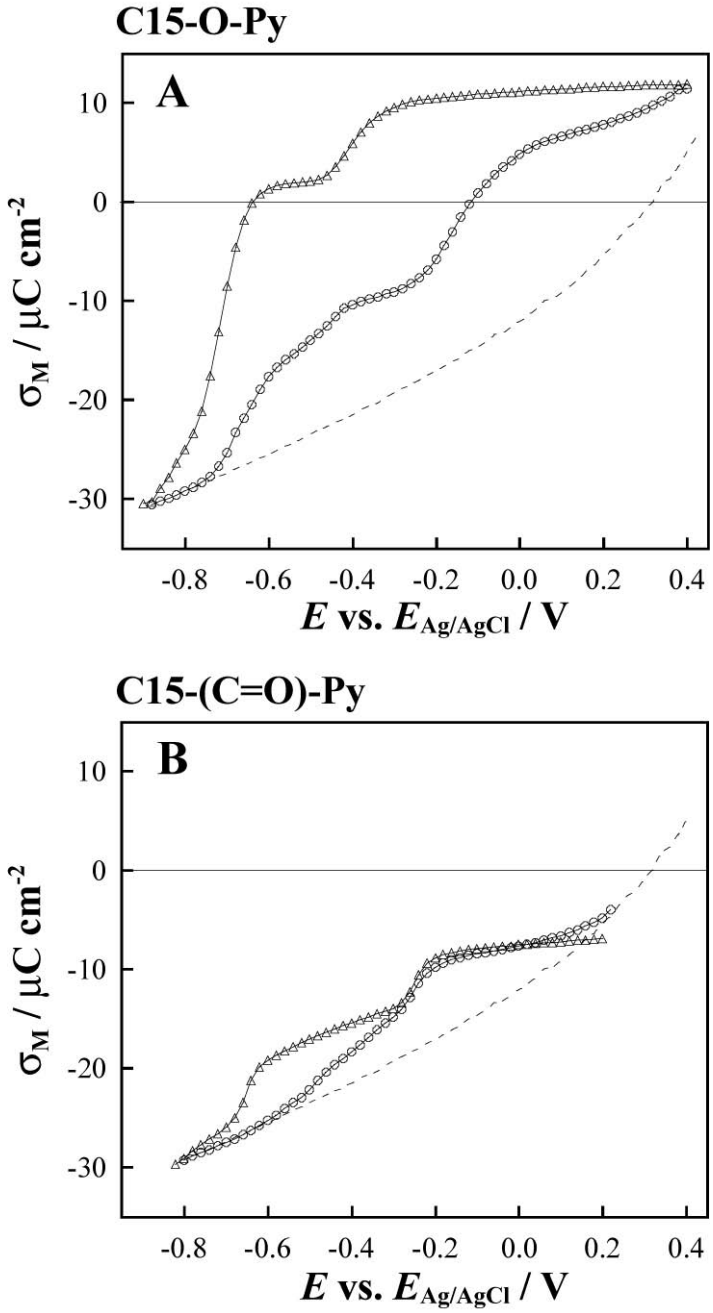
C15-O-Py
A
10
0
-10
-20
-30
σ_M / μC cm^{-2}
-0.8
-0.6
-0.4
-0.2
0.0
0.2
0.4
E vs. $E_{Ag/AgCl}$ / V
C15-(C=O)-Py
B
10
0
-10
-20
-30
σ_M / μC cm^{-2}
-0.8
-0.6
-0.4
-0.2
0.0
0.2
0.4
E vs. $E_{Ag/AgCl}$ / V

Fig. 4.

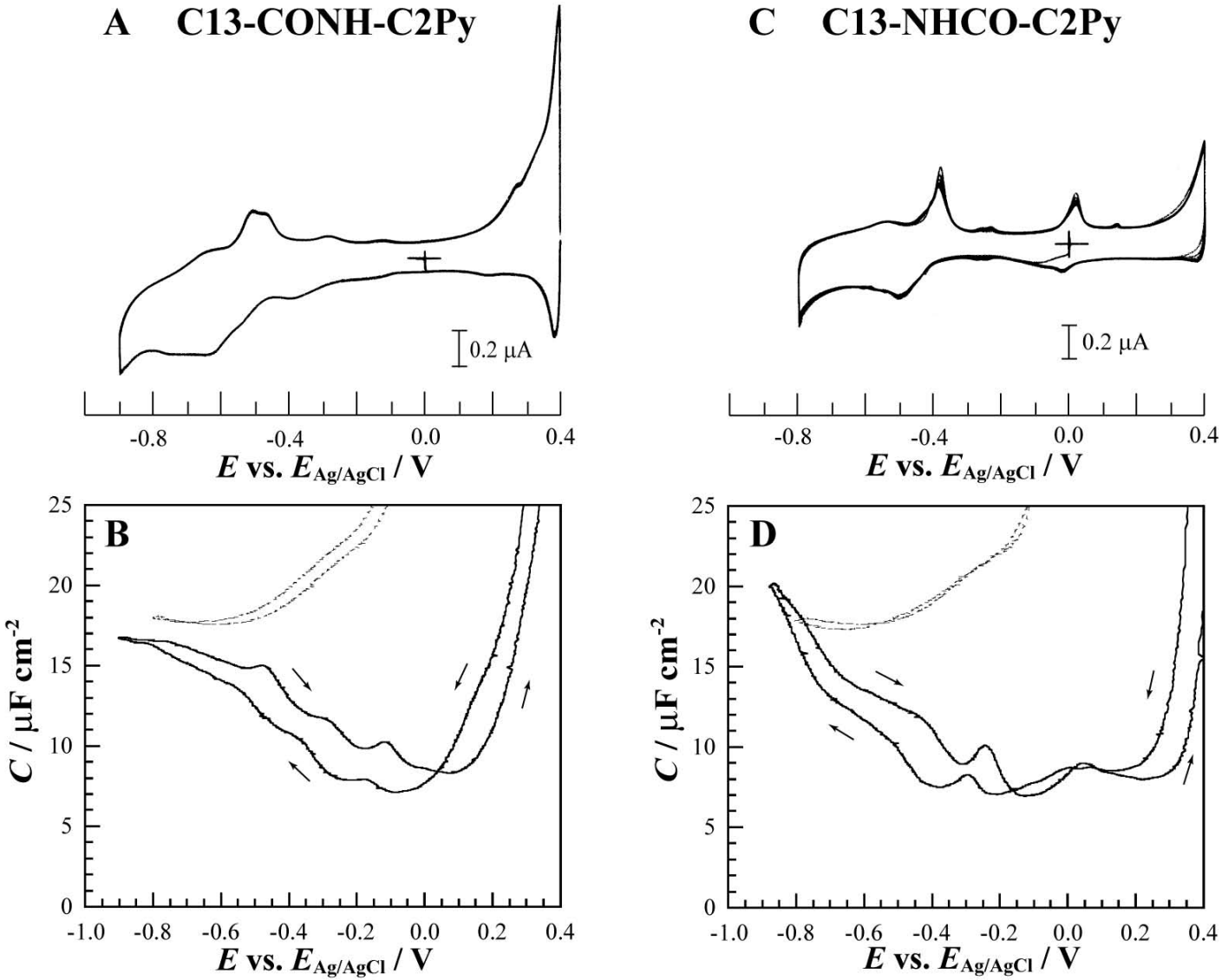
A C13-CONH-C2Py
C C13-NHCO-C2Py
0.2 μA
0.2 μA
-0.8 -0.4 0.0 0.4
E vs. E Ag/AgCl / V
B
D
C / μF cm-2
0 5 10 15 20 25
-1.0 -0.8 -0.6 -0.4 -0.2 0.0 0.2 0.4
E vs. E Ag/AgCl / V

Fig. 5.

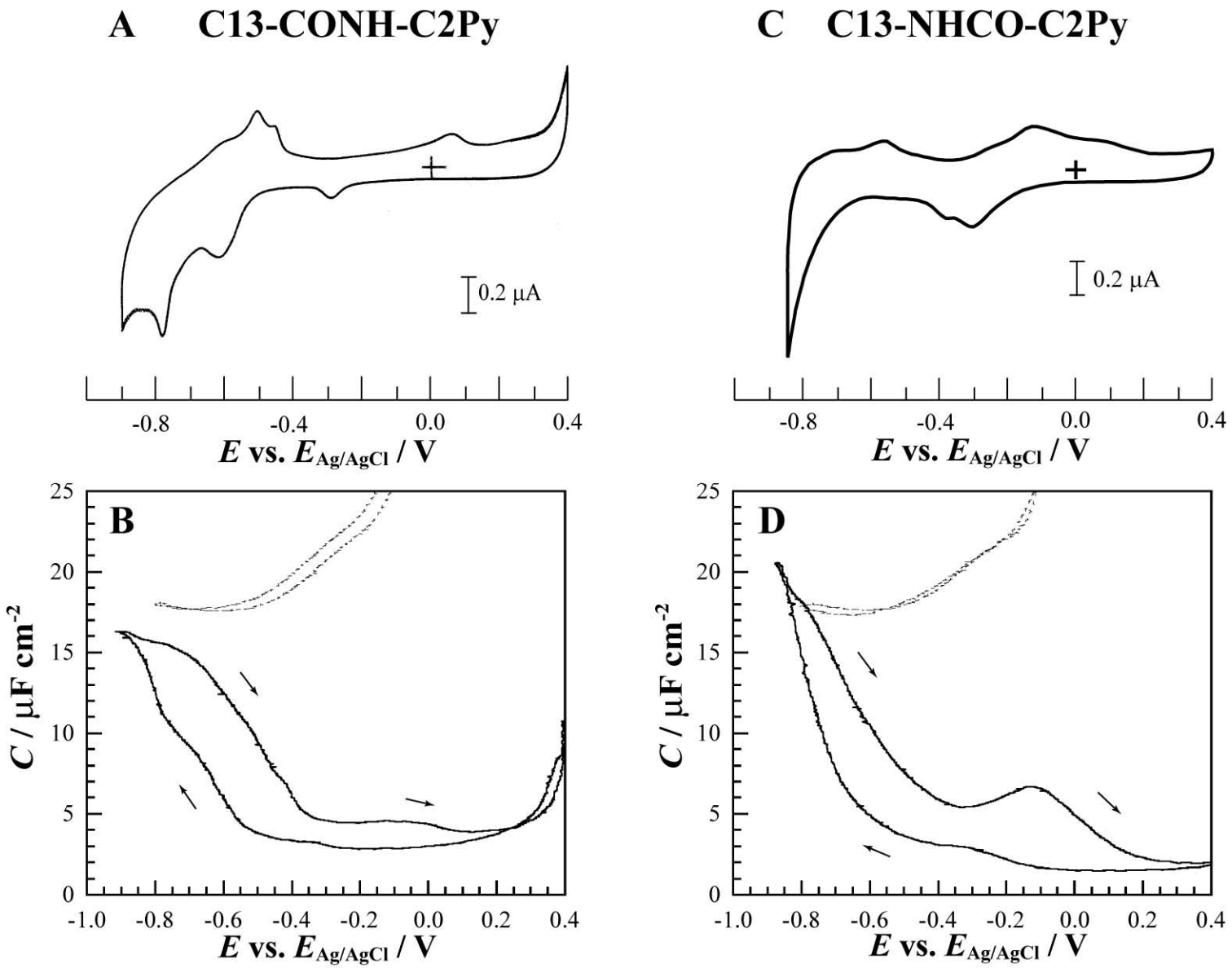
A C13-CONH-C2Py
0.2 μA
-0.8 -0.4 0.0 0.4
E vs. E Ag/AgCl / V
C C13-NHCO-C2Py
0.2 μA
-0.8 -0.4 0.0 0.4
E vs. E Ag/AgCl / V
B
C / μF cm-2
0 5 10 15 20 25
-1.0 -0.8 -0.6 -0.4 -0.2 0.0 0.2 0.4
E vs. E Ag/AgCl / V
D
C / μF cm-2
0 5 10 15 20 25
-1.0 -0.8 -0.6 -0.4 -0.2 0.0 0.2 0.4
E vs. E Ag/AgCl / V

Fig. 6.

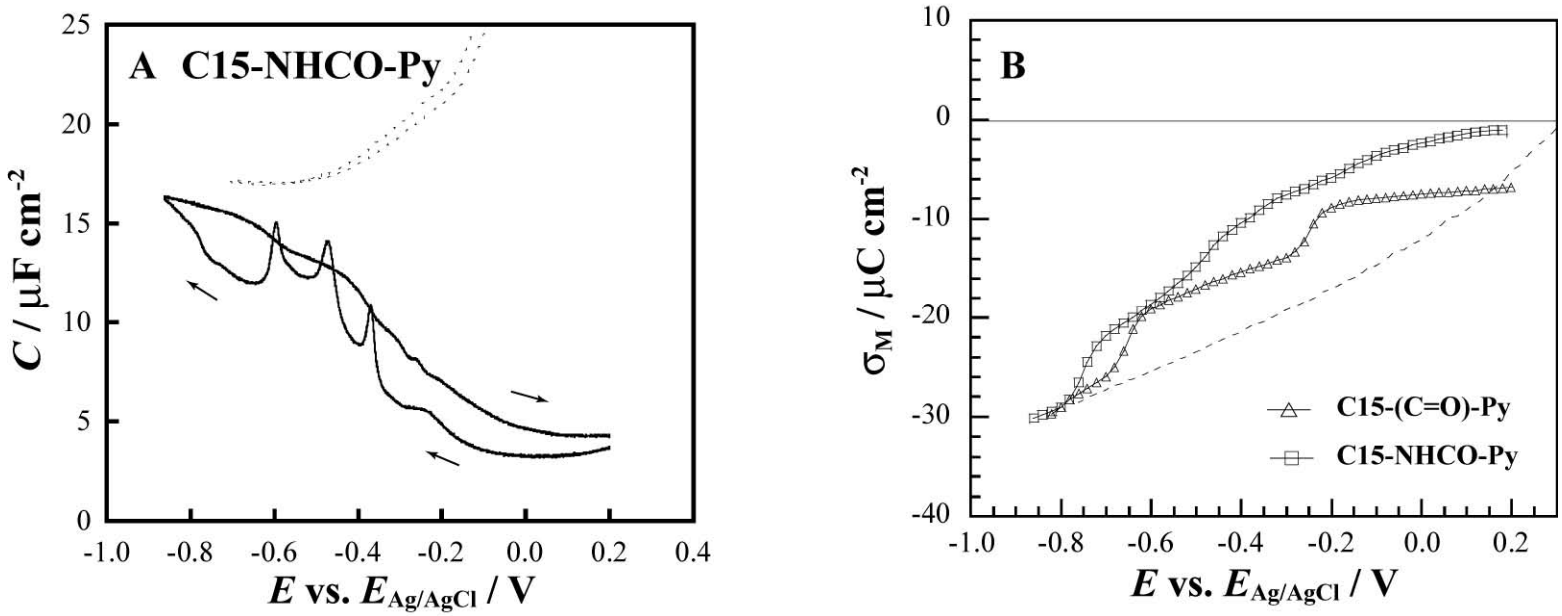
A C15-NHCO-Py
C / μF cm-2
E vs. EAg/AgCl / V
B
σM / μC cm-2
C15-(C=O)-Py
C15-NHCO-Py
E vs. EAg/AgCl / V

Fig. 7.